Sub-barrier Fusion Cross Sections: Role of Pauli Blocking and Isospin Asymmetry*

Weiwen Deng (邓玮雯)[1] Kaixuan Cheng (程凯旋)[2] Chang Xu (许昌)[1†]

[1]School of Physics, Nanjing University, Nanjing 210093, China
[2]School of Physics, Henan Normal University, Xinxiang 453007, China

Abstract: Heavy-ion fusion reaction is relevant to a number of important issues not only in stellar environment but also in the synthesis of new nuclides and superheavy elements. In this work, the role of Pauli blocking and isospin effect in sub-barrier fusion reactions is investigated within the well established coupled-channels method. An isospin-dependent Pauli blocking potential is proposed to better address the deep sub-barrier fusion hindrance problem. It is found that the Pauli blocking effect manifests itself strongly for isospin symmetric targets and is reduced for targets with large isospin asymmetries. The agreement between experimental and theoretical fusion cross sections is improved for both ^{12}C-target and ^{16}O-target systems.

Keywords: fusion hindrance, coupled-channels method, isospin effect

DOI: **CSTR:**

I. INTRODUCTION

Fusion process at sub-barrier energy region is of crucial importance for a number of interesting issues in both nuclear physics and astrophysics [1, 2]. By clarifying the details of fusion dynamics, the present understanding of astrophysical process such as carbon burning and oxygen burning, etc., could be further improved [3−5]. Fusion reactions also play an important role in the synthesis of new nuclides and superheavy elements [6−8]. Although substantial progress has been made using the cold fusion and hot fusion reactions, it remains a challenge to produce heavier elements as the fusion process is, in general, strongly blocked by both Coulomb barrier and Pauli repulsion. One of the examples which has received particular attention is the hindrance of fusion far below the Coulomb barrier [9−11], that is, the unexpected falloff in the measured fusion excitation functions of systems ^{58}Ni + ^{58}Ni, ^{90}Zr + ^{92}Zr, ^{60}Ni + ^{89}Y, ^{64}Ni + ^{64}Ni, etc., has been observed, and thus brings new challenge for both theoretical description and experimental observation [12−14].

Fusion at deep sub-barrier energies provides an effective probe for the details of internal part of the nucleus-nucleus (NN) potential. Theoretical efforts have been devoted to interpreting the fusion hindrance phenomena by refining the internal part of the NN interactions. For example, a large diffuseness parameter in the Woods-Saxon form of NN potential is employed to fit the experimental data [15−17], indicating the necessity of refining the inner part of conventional Woods-Saxon parametrization. Similarly, a calibrated repulsive core in the NN potential was proposed in Ref. [18] in order to simulate the effect of nuclear incompressibility in the inner region, which yields a good agreement between the theory and the fusion data. Moreover, the density-constrained time-dependent Hartree-Fock theory has been applied to describe hindrance problem where the Pauli energy contribution to the nucleus-nucleus interaction is taken into account [19, 20]. Recently, inspired by the inverse process of α-cluster decay [21−23], a Pauli blocking potential derived from microscopic in-medium wave functions has been incorporated into the coupled-channels method to better account the repulsive core and hindrance phenomena [24, 25]. Both the α-induced and $n\alpha$-induced fusion reactions are analyzed in detail, in which the shallow ``pocket'' in the inner region resulted from Pauli blocking is found to play a non-trivial role in explaining the abrupt decrease of quantum tunneling probability during fusion process [24−27].

Despite much effort has been paid to hindrance phenomena at extreme sub-barrier energies, the density overlapping process of the projectile-target system and the Pauli blocking involved in fusion process are still not fully understood. In addition, there is a clear experimental observation of the dependence of sub-barrier suppres-

Received 17 October 2024; Accepted 23 December 2024

* This work is supported by the National Natural Science Foundation of China (Grant No. 12275129 and No. 12105080) and the Fundamental Research Funds for the Central Universities (Grant No. 020414380209)

† E-mail: cxu@nju.edu.cn

sion on the structure of the interacting nuclei [10]. Especially, the nuclear isospin effect is considered to play a role in the Pauli blocking process after two nuclei contact and affects the onset of the sub-barrier fusion hindrance [28−31]. A better understanding of nuclear isospin dependence of the fusion hindrance for very neutron-rich nuclei will be helpful for the synthesis of superheavy nuclei using radioactive beams [32]. In this work, we propose an improved Pauli blocking potential $V_{Pi}^{n\alpha}$ with explicit isospin asymmetries and perform coupled-channels calculations for a number of systems, namely, ^{16}O + ^{72,74}Ge, ^{92}Zr, ^{142,144}Nd, ^{144,148}Sm, ^{208}Pb and ^{12}C + ^{198}Pt, ^{208}Pb. The comparison between different isospin asymmetric systems may shed more light on the fusion hindrance phenomena and the isospin effect in low-energy nuclear reactions involving exotic nuclei far from the stability line.

The rest of this paper is organized as follows. In Sec.2, the coupled-channels formalism together with the double-folding potential are presented, and the construction of the isospin-dependent Pauli blocking potential is explained in detail. In Sec.3, we firstly display the Pauli potentials in different fusion systems and then compare the calculated total and partial fusion cross sections, the astrophysical S factors, as well as the mean square deviation from experimental data. Finally, the isospin effect in different fusion systems is discussed. In Sec.4, a summary is given.

II. THEORETICAL FRAMEWORK OF COUPLED-CHANNELS (CC) METHOD

The well-established CC model has been widely adopted in the calculations of fusion reactions [17, 33−35], which addresses the coupling between nuclear intrinsic motions and the relative motion of the colliding nuclei [1, 12]. By imposing the isocentrifugal approximation, the angular momentum of the relative motion is replaced by the total angular momentum J and the coupled-channels Schrödinger equations can be written as

$$\left[-\frac{\hbar^2}{2\mu}\frac{d^2}{dR^2}+\frac{J(J+1)\hbar^2}{2\mu R^2}+V(R)+\epsilon_n-E\right]u_n(R)+\sum_m V_{nm}(R)u_m(R)=0, \tag{1}$$

where E is the bombarding energy in the center-of-mass frame and ϵ_n is the excitation energy of the n-th channel. J is the total angular momentum of the fusion system. $u_n(R)$ is the radial wave function of the n-th channel of the fusion system. $V(R)$ is the total potential which consists of Coulomb and nuclear interactions, i.e., $V(R) = V_C(R) + V_N(R)$. $V_C(R)$ and $V_N(R)$ are obtained by double-folding procedure that will be discussed in section.2.1. Matrix elements of the coupling Hamiltonian V_{nm} are given by the sum of V_{nm}^N and V_{nm}^C, which represent the nuclear and Coulomb components, respectively. And the matrix elements will be discussed in section.2.2.

A. Projectile-target potentials and construction of Pauli blocking potentials

The Michigan-3-Yukawa (M3Y) double-folding potential [36] is suited for the description of fusion cross sections, which incorporates the nucleon distributions of the reacting nuclei [37]. However, the M3Y potential is known to overestimate the experimental fusion cross sections at deep sub-barrier energies. A microscopic Pauli blocking potential obtained by solving the in-medium four-nucleon wave equation [21] can improve greatly the exchange term in the standard M3Y potential. Here we propose an isospin-dependent Pauli potential $V_{Pi}^{n\alpha}$ based on our previous calculations [25]. The M3Y+Pauli double-folding nucleus-nucleus potential $V_N(R)$ and the Coulomb potential $V_C(R)$ are defined as follows,

$$V_N(\mathbf{R}) = \int d\mathbf{r_1}d\mathbf{r_2}\rho_1(\mathbf{r_1})\rho_2(\mathbf{r_2})g(|\mathbf{s}|) + V_{Pi}^{n\alpha}(\mathbf{R}), \tag{2}$$

$$V_C(\mathbf{R}) = \int d\mathbf{r_1}d\mathbf{r_2}\frac{e^2}{|\mathbf{s}|}\rho_{1p}(\mathbf{r_1})\rho_{2p}(\mathbf{r_2}), \tag{3}$$

where $\mathbf{R}$ is the separation of the centers of mass of two reacting nuclei and $|\mathbf{s}|$ ($\mathbf{s} = \mathbf{R} - \mathbf{r_1} + \mathbf{r_2}$) is the distance between a nucleon in the target and a nucleon in the projectile. ρ_1 denotes the nucleon density distribution of the target, i.e., the sum of proton and neutron density. And ρ_2 is the nucleon density distribution of the projectile. ρ_{1p} and ρ_{2p} are the proton density distributions of the two participants. The density-dependent nucleon-nucleon interaction $g(|\mathbf{s}|)$ follows the form

$$g(|\mathbf{s}|) = \left[c_1\frac{\exp(-4s)}{4s} - c_2\frac{\exp(-2.5s)}{2.5s}\right]F(\rho), \tag{4}$$

where the multiplier $F(\rho)$ is given by $F(\rho) = C[1+\alpha\exp(-\beta\rho)]$ and the values of the parameters C, α and β are from Ref. [38]. We focus on the $n\alpha$ + target fusion systems, namely, ^{12}C group and ^{16}O group. For the ^{12}C group, the fitted strength of the Yukawa interactions is $c_1 = 9989$ MeV·fm and $c_2 = 3023$ MeV·fm, respectively. The fitted strength $c_1 = 2954.5$ MeV·fm and $c_2 = 1554$ MeV·fm is used for the ^{16}O group. The neutron ($k = n$) and proton ($k = p$) density distributions of the target nuclei are taken as the standard Fermi form [39],

$$\rho_{1k}(r) = \frac{\rho_{0k}}{1+\exp\left(\frac{r-C_k}{a_k}\right)}, \tag{5}$$

where C_k and a_k are the half-density radius and diffuseness, respectively, and their values are taken from Ref. [40]. ρ_{0k} is the normalization coefficient. The modified Gaussian form is used for the density distributions of projectiles, where the parameters ω and γ are obtained by fitting the corresponding root-mean-square (rms) radii and ρ_{02} is determined by integrating the density distribution equivalent to the corresponding mass number [41, 42]

$$\rho_2(r) = \rho_{02}\left(1+\omega r^2\right)\exp\left(-\gamma r^2\right). \tag{6}$$

In order to relate the density distribution of projectile ρ_p to that of the α particle ρ_α, an α-cluster distribution function inside the nucleus, $\rho_c(r)$, was proposed [25]

$$\rho_2(\mathbf{r}) = \int \rho_c(\mathbf{r}')\rho_\alpha(|\mathbf{r}-\mathbf{r}'|)d\mathbf{r}', \tag{7}$$

in which the distribution of α particle is described as the widely used Gaussian form [43]

$$\rho_\alpha(r) = \rho_{0\alpha}\exp\left(-\lambda r^2\right). \tag{8}$$

Combining Eqs.(6), (7) and (8), by using the Fourier transform technique [43], one can obtain the distribution function of α clusters

$$\rho_c(r) = \rho_{0c}\left(1+\mu r^2\right)\exp\left(-\xi r^2\right), \tag{9}$$

in which

$$\eta = \lambda-\gamma, \quad \xi = \gamma\lambda/\eta, \quad \mu = \frac{2\omega\lambda^2}{\eta(2\eta-3\omega)}. \tag{10}$$

From the above discussion one gives the $n\alpha$ Pauli blocking potential by utilizing a single folding procedure

$$V_{Pi}^{n\alpha}(\mathbf{R}) = \int \rho_c(\mathbf{r}')\,V_{pi}^{\alpha}(\mathbf{R}+\mathbf{r}')d\mathbf{r}', \tag{11}$$

where V_{pi}^{α} is the isospin-dependent Pauli blocking potential between the target and a single α particle. For homogeneous systems, the Pauli blocking potential for α projectile (2n+2p) is microscopically obtained by solving the in-medium Schrödinger equations [21−23]. With the Jacobian momenta $\mathbf{p}_1=\mathbf{P}/4+\mathbf{k}/2+\mathbf{k}_{12}, \mathbf{p}_2=\mathbf{P}/4+\mathbf{k}/2-\mathbf{k}_{12}$, $\mathbf{p}_3=\mathbf{P}/4-\mathbf{k}/2+\mathbf{k}_{34}, \mathbf{p}_4=\mathbf{P}/4-\mathbf{k}/2-\mathbf{k}_{34}$, the in-medium Schrödinger equation is given by

$$\begin{aligned}&\frac{\hbar^2}{2m}[k^2+2k_{12}^2+2k_{34}^2]\tilde{\varphi}^{\rm intr}(\mathbf{k},\mathbf{k}_{12},\mathbf{k}_{34};\mathbf{P}) + \int \frac{d^3k'}{(2\pi)^3}\frac{d^3k'_{12}}{(2\pi)^3}\frac{d^3k'_{34}}{(2\pi)^3}\tilde{V}_4(\mathbf{k},\mathbf{k}_{12},\mathbf{k}_{34};\mathbf{k}',\mathbf{k}'_{12},\mathbf{k}'_{34};\mathbf{P})\tilde{\varphi}^{\rm intr}(\mathbf{k}',\mathbf{k}'_{12},\mathbf{k}'_{34};\mathbf{P})\\ &= \tilde{W}(\mathbf{P})\tilde{\varphi}^{\rm intr}(\mathbf{k},\mathbf{k}_{12},\mathbf{k}_{34};\mathbf{P}),\end{aligned} \tag{12}$$

where the centroid of α-cluster is considered to be at rest (**P**=0) in homogeneous nuclear matter. The effective in-medium interaction $\tilde{V}_4(\mathbf{k},\mathbf{k}_{12},\mathbf{k}_{34};\mathbf{k}',\mathbf{k}'_{12},\mathbf{k}'_{34};\mathbf{P})$ contains the external mean field $\tilde{V}_4^{\rm ext}$ felt by the α projectile as well as the intrinsic nucleon-nucleon interaction $\tilde{V}_4^{\rm intr}$ modified by the Pauli blocking

$$\begin{aligned}\tilde{V}_4^{\rm intr}(\mathbf{k},\mathbf{k}_{12},\mathbf{k}_{34};\mathbf{k}',\mathbf{k}'_{12},\mathbf{k}'_{34};\mathbf{P}) &= \tilde{V}_4^{\rm intr}(\mathbf{p}_1,\mathbf{p}_2,\mathbf{p}_3,\mathbf{p}_4;\mathbf{p}'_1,\mathbf{p}'_2,\mathbf{p}'_3,\mathbf{p}'_4) = \tilde{V}_{12}^{\rm intr}+\tilde{V}_{13}^{\rm intr}+\tilde{V}_{14}^{\rm intr}+\tilde{V}_{23}^{\rm intr}+\tilde{V}_{24}^{\rm intr}+\tilde{V}_{34}^{\rm intr}\\ &= \Theta(p_1-k_F)\Theta(p_2-k_F)V_{N-N}(\mathbf{p}_1,\mathbf{p}_2;\mathbf{p}'_1,\mathbf{p}'_2)\delta(\mathbf{p}_3-\mathbf{p}'_3)\delta(\mathbf{p}_4-\mathbf{p}'_4)+\text{five permutations},\end{aligned} \tag{13}$$

with the nucleon-nucleon interaction defined as a Gaussian form factor

$$\begin{aligned}V_{N-N}(\mathbf{p}_1,\mathbf{p}_2;\mathbf{p}'_1,\mathbf{p}'_2) = \lambda e^{-\frac{(\mathbf{p}_1-\mathbf{p}_2)^2}{4\gamma^2}}e^{-\frac{(\mathbf{p}'_1-\mathbf{p}'_2)^2}{4\gamma^2}}\\ \times\delta(\mathbf{p}_1+\mathbf{p}_2-\mathbf{p}'_1-\mathbf{p}'_2),\end{aligned} \tag{14}$$

and the states below the Fermi sphere $k_F=(3\pi^2\rho_B/2)^{1/3}$ are blocked out. ρ_B represents the baryon density, defined as $\rho_B=\rho_n+\rho_p$. The $\tilde{W}(\mathbf{P})$ is decomposed into $\tilde{W}(\mathbf{P})=\tilde{W}^{\rm ext}(\mathbf{P})+\tilde{W}^{\rm intr}(\mathbf{P})$. By performing the variational calculation for the intrinsic part, the in-medium equation can be solved with a Gaussian ansatz

$$\begin{aligned}\tilde{\varphi}^{\rm intr}(\mathbf{p}_1,\mathbf{p}_2,\mathbf{p}_3,\mathbf{p}_4) = \frac{1}{\sqrt{N}}\varphi_{\tau_1}(\mathbf{p}_1)\varphi_{\tau_1}(\mathbf{p}_2)\varphi_{\tau_1}(\mathbf{p}_3)\varphi_{\tau_1}(\mathbf{p}_4)\\ \times\delta(\mathbf{p}_1+\mathbf{p}_2+\mathbf{p}_3+\mathbf{p}_4)\end{aligned} \tag{15}$$

with $\varphi_\tau(\mathbf{p}) = e^{-\frac{\mathbf{p}^2}{2\alpha}}\Theta\left[p-k_{\rm F}\right]$. We have to evaluate the normalization factor N of the trial function as well as the kinetic and potential energy. For each density ρ_B, the minim-

um of the intrinsic energy $\tilde{W}^{\rm intr}(\rho_B)$ has to be found with the ansatz and the Pauli blocking for α projectile embedded in nuclear medium is taken into account. Thus the Pauli blocking potential is obtained for homogeneous nuclear matter from

$$\tilde{W}^{intr}(\rho_B) = E_\alpha^{(0)} + \tilde{W}^{Pauli}(\rho_B), \tag{16}$$

where $E_\alpha^{(0)} = -28.3$ MeV is the bound-state energy for α particles in the zero-density limit. Here a fit formula is given to simulate the result of microscopic calculation within the variational approach,

$$\tilde{W}^{\rm Pauli}(\rho_B) = 4515.9\rho_B - 100935\rho_B^2 + 1202538\rho_B^3. \tag{17}$$

For imbalanced systems, it is rather difficult to perform variational calculations. Recently, we have performed microscopic calculations for isospin asymmetric systems [44]. It is found that Pauli blocking potential is reduced for imbalanced systems. In the present work we improve the Pauli blocking potential by including a new term related to the isospin asymmetry of the target, i.e.,

$$V_{Pi}^{\alpha}\left(\rho_1(r)\right) = \tilde{W}^{Pauli}(\rho_1(r))/\left(1+\delta(r)^2\right), \tag{18}$$

where $\delta(r)$ is the isospin asymmetry defined as $\delta(r) = (\rho_{1n}(r) - \rho_{1p}(r))/(\rho_{1n}(r) + \rho_{1p}(r))$.

B. Vibrational coupling matrix elements and coupling parameters

Let us now discuss the explicit form of the coupling Hamiltonian for heavy-ion fusion reactions. It has been demonstrated that the low-lying collective excitations of the colliding nuclei during fusion have a significant impact on the fusion cross section by modifying the potential between the colliding nuclei, especially at sub-barrier colliding energies [2, 45−47]. The surface vibration of the colliding nuclei, as a type of collective excitations, is considered in our calculation. The Hamiltonian for the coupling of the relative motion to the surface vibration of the nucleus is introduced by considering the change of the nucleus radius in the potential. Taking the target as an example, the change of its radius considering the deformation during fusion can be expressed by a dynamical operator $\hat{O}$,

$$R_T \to R_T + \hat{O}. \tag{19}$$

The surface vibration of the nucleus is approximated by a harmonic oscillator, thus the dynamical operator is given by

$$\hat{O} = \frac{\beta_\lambda}{\sqrt{4\pi}} R_T \left(a_{\lambda 0}^\dagger + a_{\lambda 0}\right), \tag{20}$$

where λ and β_λ are the multipolarity of the vibrational mode and the corresponding deformation parameter, respectively. $a_{\lambda 0}^\dagger$ and $a_{\lambda 0}$ denote the creation and annihilation operators of the phonon, respectively. Hence the matrix element of this operator between the n-phonon state $|n\rangle$ and the m-phonon state $|m\rangle$ is obtained,

$$O_{nm} = \frac{\beta_\lambda}{\sqrt{4\pi}} R_T \left(\sqrt{m}\delta_{n,m-1} + \sqrt{n}\delta_{n,m+1}\right). \tag{21}$$

By numerically diagonalizing the matrix $\hat{O}$, $\hat{O}|\alpha\rangle = \lambda_\alpha|\alpha\rangle$, where λ_α and $|\alpha\rangle$ are the eigenvalues and eigenvectors of $\hat{O}$, the nuclear coupling matrix elements are evaluated as

$$\begin{aligned} V_{nm}^N(R) &= \langle n \left| \tilde{V}_N\left(R, \hat{O}_\lambda\right) \right| m\rangle - V_N(R)\delta_{n,m} \\ &= \sum_\alpha \langle n \mid \alpha\rangle\langle\alpha \mid m\rangle \tilde{V}_N(R, \lambda_\alpha) - V_N(R)\delta_{n,m}, \end{aligned} \tag{22}$$

where $\tilde{V}_N\left(R, \hat{O}_\lambda\right) = V_N\left(R - \hat{O}_\lambda\right)$.

The Coulomb coupling matrix elements V_{nm}^C are calculated by the linear coupling approximation [12]

$$V_{nm}^C(R) = \frac{\beta_\lambda}{\sqrt{4\pi}} \frac{3}{2\lambda+1} Z_P Z_T e^2 \frac{R_T^\lambda}{R^{\lambda+1}} \left(\sqrt{m}\delta_{n,m-1} + \sqrt{n}\delta_{n,m+1}\right). \tag{23}$$

Again, the total coupling matrix element is determined by adding the values of V_{nm}^N and V_{nm}^C. Detailed structure inputs for describing the excitation of low-lying states in fusing partners are listed in Table 1.

C. Calculation of fusion cross sections

The total fusion cross section is obtained by summing the partial fusion cross sections,

$$\sigma_{\rm fus}(E) = \frac{\pi}{k_0^2} \sum_J (2J+1) P_J(E), \tag{24}$$

in which the penetrability P_J is given by

$$P_J(E) = \sum \frac{k_n(R_{\rm min})}{k_0} |T_n|^2, \tag{25}$$

where $k_n(R_{\rm min})$ is the local wave number for the n-th channel at the minimum position of the Coulomb pocket, and k_0 is that for the entrance channel. In CCFULL, coupled-channels equations are solved by using the incoming wave boundary condition (IWBC), and integrating the equations directly with the modified Numerov

Table 1. The deformation parameters β_λ of vibrational states along with their corresponding excitation energies E_x used in the coupled channel calculations for different nuclei. λ^π denotes the multipolarity and parity of a state.

Nuclei	λ^π	E_x(MeV)	β_λ	References
^{12}C	2^+	4.440	0.590	[48]
^{16}O	3^-	6.130	0.729	[18]
	2^+	6.917	0.349	[18]
^{28}Si	2^+	1.779	-0.407	[49]
	3^-	6.879	0.401	[49]
^{30}Si	2^+	2.235	0.330	[50]
	3^-	5.488	0.275	[50]
^{72}Ge	2^+	0.834	0.240	[51]
^{74}Ge	2^+	0.596	0.285	[51]
^{92}Zr	2^+	0.934	0.101	[52]
	3^-	2.340	0.174	[52]
^{100}Mo	2^+	0.536	0.230	[49]
	3^-	1.908	0.220	[49]
^{142}Nd	2^+	1.575	0.092	[53]
	3^-	2.084	0.127	[53]
^{144}Nd	2^+	0.696	0.120	[54]
	4^+	1.314	0.060	[54]
^{144}Sm	2^+	1.660	0.087	[52]
	3^-	1.810	0.151	[52]
^{148}Sm	2^+	0.555	0.140	[55]
	3^-	1.160	0.190	[55]
^{198}Pt	2^+	0.407	0.110	[56]
	3^-	1.500	0.100	[56]
^{208}Pb	3^-	2.615	0.111	[18]
	5^-	3.198	0.059	[18]

method. The transmission coefficient T_n of the n-th channel satisfies:

$$u_m(R) = \sum_n T_n \chi_{nm}(R), \tag{26}$$

where $\chi_{nm}(R)$ is the wave function of the m-th channel obtained from $u_n(R)$.

III. RESULTS OF FUSION CROSS SECTIONS AND DISCUSSION ON THE ISOSPIN EFFECT

We adopt ^{16}O + ^{72,74}Ge as a representative example. The nucleus-nucleus potentials calculated with and without the isospin dependent term, as well as the nucleon density distributions of targets are displayed in Fig.1. For both the fusion systems, the isospin effect leads to lower Pauli blocking potentials, in turn, the deeper pockets and narrower barriers compared with the isospin-independent ones. For the ^{16}O + ^{74}Ge fusion reaction with larger isospin asymmetry, the variation of the minimum energy of the pocket, $\Delta V_{min} = 1.96$ MeV, is larger than that for the ^{16}O + ^{72}Ge system, $\Delta V_{min} = 1.12$ MeV. Note that the Coulomb repulsion of the two systems is identical, so the difference between the ΔV_{min} is mainly originated from the Pauli blocking potential.

Similar phenomenon can also be found in other systems, as shown in Fig.2. For all the ^{16} O-target systems, ΔV_{min} as a function of the isospin asymmetry of the target $I = (N-Z)/A$, is given in the insert. It is shown that the isospin effect is more evident for the target with larger I, and the variation of the minimum pocket energy, ΔV_{min} increases linearly with I. For instance, ^{16}O + ^{208}Pb shows the greatest variation of the minimum energy. Note that the barrier penetration probability has an exponential dependence on the barrier properties. A small change of the pocket position by the isospin effect will result in a non-negligible role in the theoretical fusion cross sections especially at sub-barrier energies.

Fusion excitation functions of ^{16}O + ^{72,74}Ge and ^{16}O + ^{144,148}Sm systems are shown in Fig.3, performed by the CCFULL [57]. It is found that the experimental fusion cross sections can be reproduced well by including the isospin effect in the Pauli blocking potential, whereas the results calculated without this effect underestimate the data at sub-barrier energies, especially for the ^{144,148}Sm targets. At near and above barrier energies, there is no obvious difference between the isospin-dependent results and the isospin-independent ones. This is because at high incident energies, a compound nucleus is assumed to be formed before the two colliding nuclei strongly overlap [58], thus the Pauli blocking effect is relatively weaker. As the incident energy decreases towards sub-barrier energies, owing to the large density overlap, the Pauli blocking effect becomes increasingly important especially for isospin symmetric systems.

Detailed insights into fusion process can be obtained from angular momentum dependence of fusion cross sections. Partial fusion cross sections of the reactions ^{16}O + ^{72,74}Ge calculated at several specified experimental incident energies, namely, 32.1 MeV, 31.3 MeV for the ^{72}Ge target and 31.9 MeV, 31.1 MeV for the ^{74}Ge target, are given in Fig.4. It is clearly shown that isospin effect enhances the partial fusion cross sections. For example, the maximum partial fusion cross section at 32.1 MeV of the ^{16}O + ^{72}Ge system increases from 0.102 mb to 0.174 mb. Higher angular momentum components with $J > 12$ also contribute to the total fusion cross sections after taking into account the isospin effect.

To further explore the isospin dependence of Pauli blocking potentials, we calculate fusion cross sections of

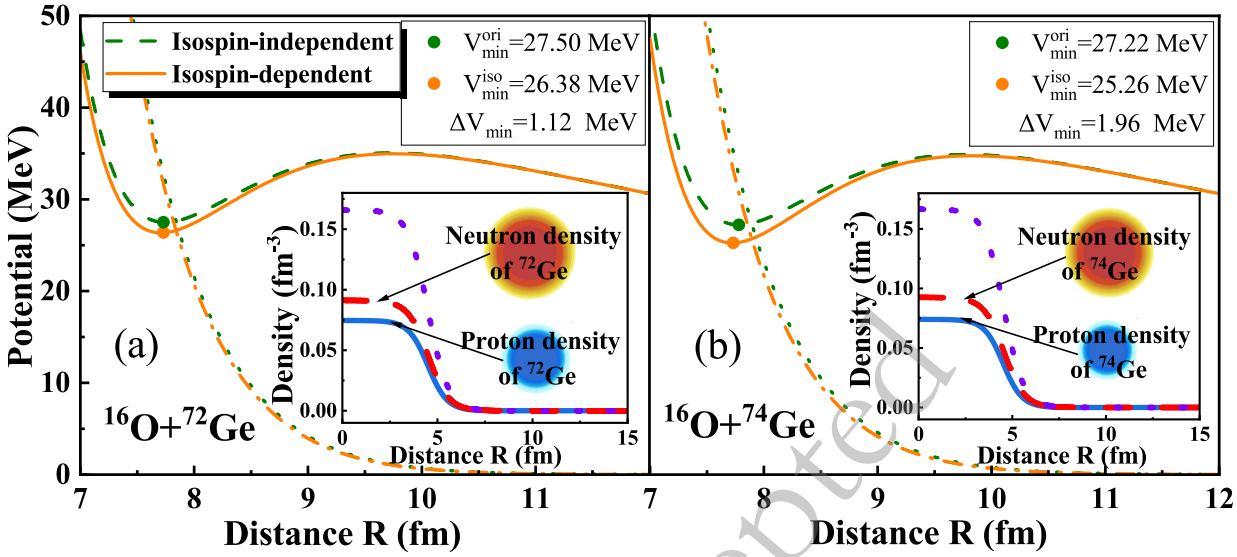

Fig. 1. (color online) (a) Potentials of fusion reaction $^{16}O+^{72}Ge$ and the nucleon density distributions of the target ^{72}Ge. The orange dot-dash line represents the Pauli blocking potential, and the orange solid line represents the total potential, calculated by including the isospin effect. The green dotted line represents the Pauli blocking potential, and the green dashed line represents the total potential, calculated without the isospin effect. The nucleon density distributions are shown in the insert, in which the red dashed line denotes the neutron density distribution, the blue solid line denotes the proton density distribution, and the violet dotted line is the sum of the neutron density and proton density of the target. (b) Potentials of fusion reaction $^{16}O+^{74}Ge$ and the nucleon density distributions of the target ^{74}Ge.

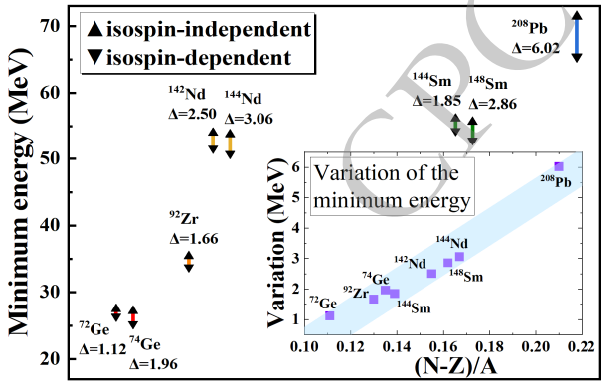

Fig. 2. (color online) Variation of the minimum pocket energy after introducing the isospin-dependent term in the Pauli blocking potential. The triangles and inverted triangles denote the minimum energies of the pockets obtained by the isospin-independent and isospin-dependent Pauli blocking potentials, respectively. For all the calculated ^{16}O-target systems, ΔV_{min} as a function of the isospin asymmetry of the target, $I=(N-Z)/A$, is given in the insert.

more systems including $^{16}O+^{92}Zr$, $^{16}O+^{208}Pb$, $^{12}C+^{198}Pt$ and $^{12}C+^{208}Pb$. The best-fit global values of the Yukawa interaction strength for the ^{16}O- and ^{12}C-induced reactions and the mean square errors (MSE) are given in Table 2. The MSE are used to get the goodness of fit for all studied systems

$$MSE=\frac{1}{N}\sum_{i=1}^{N}\left[\frac{\sigma_{exp}(E_{c.m.})-\sigma_{th}(E_{c.m.})}{\sigma_{exp}(E_{c.m.})}\right]^2, \qquad (27)$$

where σ_{th} and σ_{exp} respectively represent the theoretical and experimental total fusion cross sections and N is the number of experimental points used for fitting in each fusion system. The values of mean square errors calculated by isospin-independent and isospin-dependent Pauli blocking potentials are compared in Table 2. The MSE value of the system with the largest isospin asymmetry, $^{16}O+^{208}Pb$, improves most obviously among all the calculated fusion systems. The total MSE-values with isospin term for the ^{12}C and ^{16}O groups are found to be smaller than that without isospin term, indicating that the Pauli potentials ``felt" by the target nuclei with larger isospin asymmetries are effectively lower than the ones with smaller isospin asymmetries.

Recently, an experimental study on the sub-barrier fusion of $^{28}Si+^{100}Mo$ observed a tendency of the astrophysical S factor to develop a maximum, which would be a clear indication of hindrance [49]. It is pointed out in Ref. [49] that CC calculations performed with the best-fit Woods-Saxon potential are hard to reproduce the flat trend of S at the lowest energy. Interestingly, in the present work, it is found that the M3Y+isospin-dependent Pauli blocking essentially improved the data fit. The calculated fusion cross sections of $^{28}Si+^{100}Mo$ and the conversion to the S factor are given in Fig.5 (a). It can be

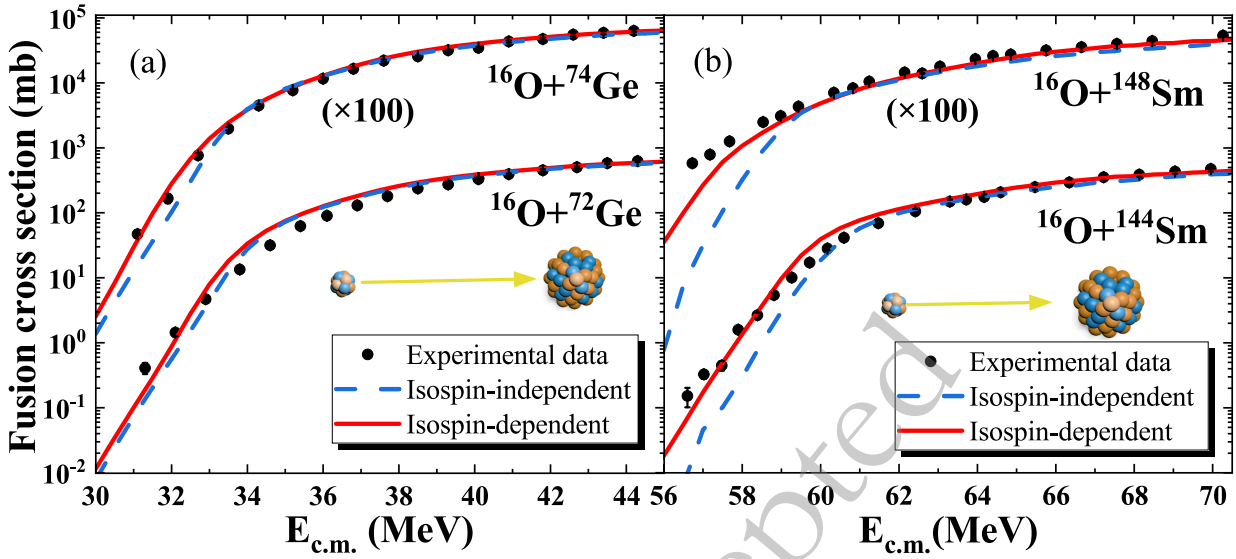

Fig. 3. (color online) (a) Comparison of the fusion cross sections of ^{16}O+^{72}Ge and ^{16}O+^{74}Ge systems calculated by using isospin-independent Pauli blocking potentials (blue dashed lines) and isospin-dependent ones (red solid lines). (b) Comparison of the fusion cross sections of ^{16}O+^{144}Sm and ^{16}O+^{148}Sm systems. Note that the results for ^{16}O+^{74}Ge and ^{16}O+^{148}Sm reactions have been multiplied by 100. Experimental data are taken from Refs. [55, 59, 60].

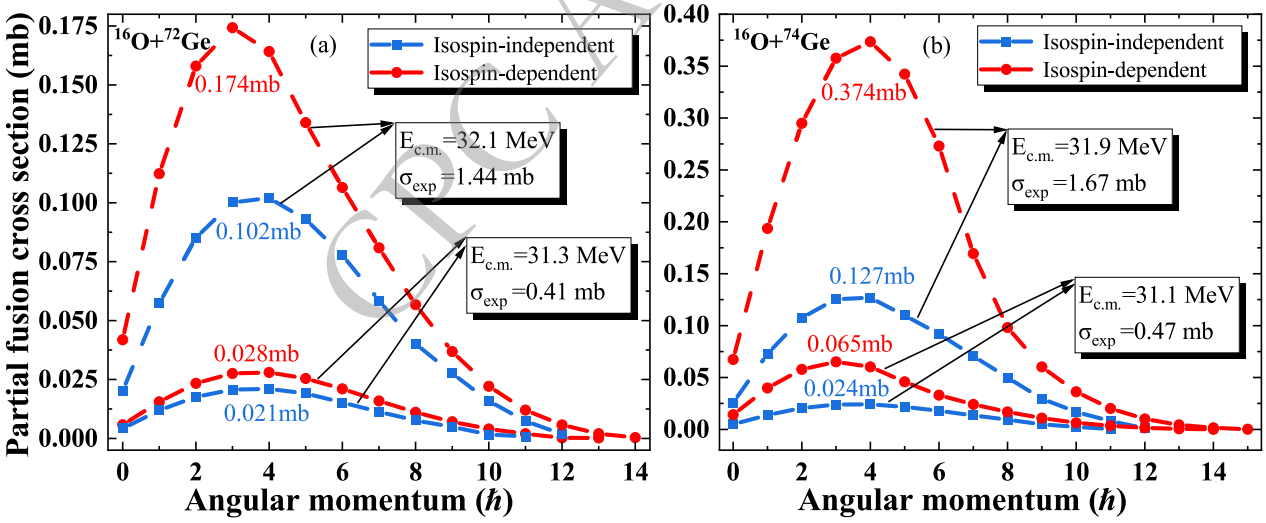

Fig. 4. (color online) (a) The partial fusion cross sections of ^{16}O+^{72}Ge system calculated by using isospin-independent Pauli blocking potentials (blue lines with squares) and isospin-dependent ones (red lines with circles). (b) The partial fusion cross sections of ^{16}O+^{74}Ge system. Experimental total fusion cross sections at specified sub-barrier energies are given in boxes [59].

seen that the M3Y+isospin-dependent Pauli blocking yields a good agreement with the experimental flat trend of S factor, especially at deep sub-barrier energies [49]. Similarly, in a lighter fusion system ^{28}Si+^{30}Si, large deviations from the experimental fusion cross sections and the optical model predictions have been observed [66]. By introducing the isospin-dependent Pauli blocking, the experimental fusion cross sections and S factors are reproduced fairly well, as shown in Fig.5 (b). We also predict the maximum of the S factor at 25.10 MeV for the ^{28}Si+^{30}Si system, and 65.44 MeV for the ^{28}Si+^{100}Mo system, whereas the isospin-independent results predict earlier onsets of the hindrance. This could be verified by future precise measurements of fusion cross sections down to deeper energies which allows locating the hindrance threshold energy.

IV. SUMMARY

We investigate the effects of Pauli blocking and isospin asymmetry on the cross sections of fusion reactions, especially at deep sub-barrier energies. The micro-

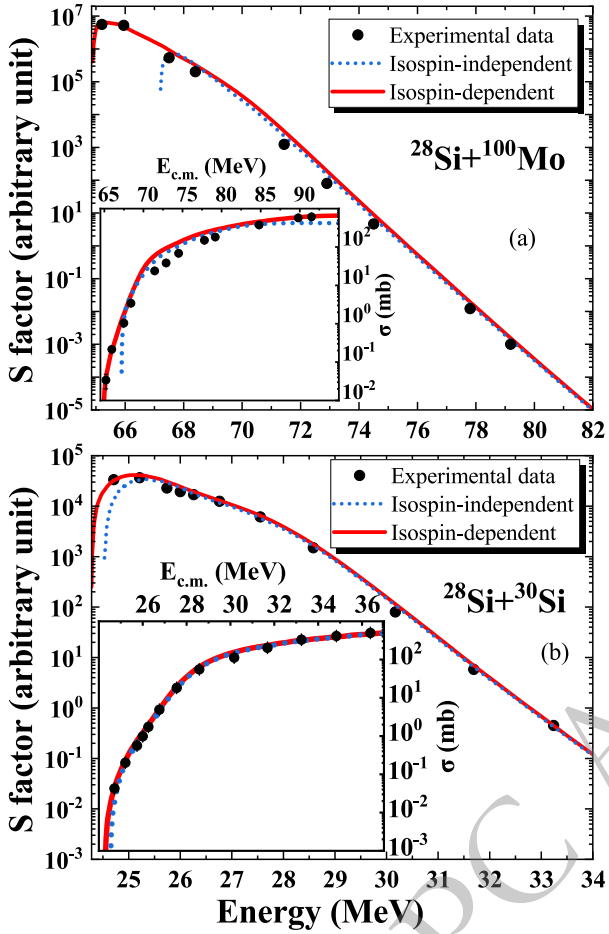

Fig. 5. (color online) (a) Excitation function and astrophysical S factor of ^{28}Si + ^{100}Mo system. The red solid lines are the isospin-dependent results, compared to the isospin-independent ones (blue dotted lines). (b) The same as (a), but for ^{28}Si + ^{30}Si system. Experimental data are taken from Refs. [49, 66].

scopic treatment of density overlapping process and Pauli blocking of isospin asymmetric fusion systems is rather difficult and should be tackled by solving complex in-medium equations. In this work, by incorporating the isospin effect, the Pauli blocking effect is found to be significant for isospin symmetric targets and slightly reduced for targets with large isospin asymmetries. For fusion systems ^{16}O + ^{72,74}Ge, ^{92}Zr, ^{142,144}Nd, ^{144,148}Sm, ^{208}Pb and systems ^{12}C + ^{198}Pt, ^{208}Pb, the involved potential pockets get deeper, and lead to enhanced fusion cross sections as compared with the isospin-independent results. The agreement between the calculated fusion cross sections and the experimental data is largely improved by considering the isospin effect. The total mean square error is reduced from 3.2776 to 2.5370 for ^{16} O-target and ^{12} C-target systems. Moreover, the calculated astrophysical S factors agree well with the data for both ^{28}Si + ^{100}Mo and ^{28}Si + ^{30}Si systems and the onset of hindrance down to lower energy region is predicted with the isospin-dependent Pauli blocking.

Table 2. Comparison of the mean square errors (MES) calculated with and without isospin term. For the ^{16}O group, the best-fit global values of c_1 and c_2 are $c_1 = 2902$ MeV·fm, $c_2 = 1575$ MeV·fm for the isospin-independent calculations, whereas $c_1 = 2954.5$ MeV·fm, $c_2 = 1554$ MeV·fm for the isospin-dependent ones. For the ^{12}C group, the best-fit values are $c_1 = 10015.5$ MeV·fm, $c_2 = 3109$ MeV·fm for the isospin-independent case, and $c_1 = 9989$ MeV·fm, $c_2 = 3023$ MeV·fm for the isospin-dependent case. The last column is the corresponding references where the experimental data are extracted from.

Systems	MSE values (Isospin-independent)	MSE values (Isospin-dependent)	Ref.
^{16}O + ^{72}Ge	0.3649	0.3165	[59]
^{16}O + ^{74}Ge	0.0520	0.0565	[59]
^{16}O + ^{92}Zr	0.2168	0.2428	[61]
^{16}O + ^{142}Nd	0.2739	0.2575	[54]
^{16}O + ^{144}Nd	0.8545	0.7659	[62]
^{16}O + ^{144}Sm	0.2490	0.2107	[60]
^{16}O + ^{148}Sm	0.2843	0.2437	[55]
^{16}O + ^{208}Pb	0.8256	0.2983	[63]
^{12}C + ^{198}Pt	0.0123	0.0087	[64]
^{12}C + ^{208}Pb	0.1443	0.1364	[65]
Total	3.2776	2.5370	

References

[1] A. B. Balantekin and N. Takigawa, Rev. Mod. Phys. **70**, 77 (1998)

[2] B. B. Back, H. Esbensen, C. L. Jiang and K. E. Rehm, Rev. Mod. Phys. **86**, 317 (2014)

[3] H. Esbensen, X. Tang, and C. L. Jiang, Phys. Rev. C **84**, 064613 (2011)

[4] L. R. Gasques, E. F. Brown, A. Chieffi, C. L. Jiang, M. Limongi, C. Rolfs, M. Wiescher, and D. G. Yakovlev, Phys. Rev. C **76**, 035802 (2007)

[5] N. Zhang, X. Wang, D. Tudor, B. Bucher, I. Burducea, H. Chen, Z. Chen, D. Chesneanu, A. Chilug, L. Gasques, *et al.*, Phys. Lett. B **801**, 135170 (2020)

[6] Z. Y. Zhang, Z. G. Gan, H. B. Yang, L. Ma, M. H. Huang, C. L. Yang, M. M. Zhang, Y. L. Tian, Y. S. Wang, M. D. Sun, *et al.*, Phys. Rev. Lett. **122**, 192503 (2019)

[7] L. Ma, Z. Y. Zhang, Z. G. Gan, H. B. Yang, L. Yu, J. Jiang, J. G. Wang, Y. L. Tian, Y. S. Wang, S. Guo, *et al.*, Phys. Rev. C **91**, 051302 (2015)

[8] M. Sun, Z. Liu, T. Huang, W. Zhang, J. Wang, X. Liu, B. Ding, Z. Gan, L. Ma, H. Yang, *et al.*, Phys. Lett. B **771**, 303 (2017)

[9] C. L. Jiang, H. Esbensen, K. E. Rehm, B. B. Back, R. V. F.

Janssens, J. A. Caggiano, P. Collon, J. Greene, A. M. Heinz, D. J. Henderson, *et al*., Phys. Rev. Lett. **89**, 052701 (2002)
[10] C. L. Jiang, K. E. Rehm, R. V. F. Janssens, H. Esbensen, I. Ahmad, B. B. Back, P. Collon, C. N. Davids, J. P. Greene, D. J. Henderson, *et al*., Phys. Rev. Lett. **93**, 012701 (2004)
[11] C. L. Jiang, B. B. Back, H. Esbensen, R. V. F. Janssens, S. Mi?icu, K. E. Rehm, P. Collon, C. Davids, J. Greene, D. Henderson, *et al*., Phys. Lett. B **640**, 18 (2006)
[12] K. Hagino and N. Takigawa, Prog. Theor. Phys. **128**, 1061 (2012)
[13] C. J. Lin, Phys. Rev. Lett. **91**, 229201 (2003)
[14] C. L. Jiang, B. B. Back, K. E. Rehm, K. Hagino, G. Montagnoli, and A. M. Stefanini, Eur. Phys. J. A **57**, 235 (2021)
[15] K. Hagino, N. Rowley, and M. Dasgupta, Phys. Rev. C **67**, 054603 (2003)
[16] K. Washiyama, K. Hagino, and M. Dasgupta, Phys. Rev. C **73**, 034607 (2006)
[17] C. J. Lin, H. M. Jia, H. Q. Zhang, F. Yang, X. X. Xu, F. Jia, Z. H. Liu, and K. Hagino, Phys. Rev. C **79**, 064603 (2009)
[18] H. Esbensen and S. Mişicu, Phys. Rev. C **76**, 054609 (2007)
[19] C. Simenel, A. S. Umar, K. Godbey, M. Dasgupta, and D. J. Hinde, Phys. Rev. C **95**, 031601 (2017)
[20] A. S. Umar, C. Simenel, and K. Godbey, Phys. Rev. C **104**, 034619 (2021)
[21] G. Röpke, P. Schuck, Y. Funaki, H. Horiuchi, Z. Ren, A. Tohsaki, C. Xu, T. Yamada, and B. Zhou, Phys. Rev. C **90**, 034304 (2014)
[22] C. Xu, Z. Ren, G. Röpke, P. Schuck, Y. Funaki, H. Horiuchi, A. Tohsaki, T. Yamada, and B. Zhou, Phys. Rev. C **93**, 011306 (2016)
[23] C. Xu, G. Röpke, P. Schuck, Z. Ren, Y. Funaki, H. Horiuchi, A. Tohsaki, T. Yamada, and B. Zhou, Phys. Rev. C **95**, 061306 (2017)
[24] K. Cheng and C. Xu, Phys. Rev. C **99**, 014607 (2019)
[25] K. Cheng and C. Xu, Phys. Rev. C **102**, 014619 (2020)
[26] K. Cheng, C. Xu, C. Ma, J. Pu, and Y. Wang, Phys. Rev. C **103**, 014613 (2021)
[27] K. Cheng, C. Xu, C. Ma, J. Pu, and Y. Wang, Chin. Phys. C **46**, 024105 (2022)
[28] C. L. Jiang, B. B. Back, R. V. F. Janssens, and K. E. Rehm, Phys. Rev. C **75**, 057604 (2007)
[29] C. L. Jiang, K. E. Rehm, H. Esbensen, R. V. F. Janssens, B. B. Back, C. N. Davids, J. P. Greene, D. J. Henderson, C. J. Lister, R. C. Pardo, *et al*., Phys. Rev. C **71**, 044613 (2005)
[30] C. L. Jiang, H. Esbensen, B. B. Back, R. V. F. Janssens, and K. E. Rehm, Phys. Rev. C **69**, 014604 (2004)
[31] R. Gumbel, C. Ross, and A. S. Umar, Phys. Rev. C **108**, L051602 (2023)
[32] W. Loveland, Phys. Rev. C **76**, 014612 (2007)
[33] Y. W. Wu, Z. H. Liu, C. J. Lin, H. Q. Zhang, M. Ruan, F. Yang, Z. C. Li, M. Trotta, and K. Hagino, Phys. Rev. C **68**, 044605 (2003)
[34] K. Hagino, N. Takigawa, M. Dasgupta, D. J. Hinde, and J. R. Leigh, Phys. Rev. C **55**, 276 (1997)
[35] G. Scamps and K. Hagino, Phys. Rev. C **92**, 054614 (2015)
[36] G. R. Satchler and W. G. Love, Phys. Rep. **55**, 183 (1979)
[37] S. Mişicu and H. Esbensen, Phys. Rev. C **75**, 034606 (2007)
[38] D. T. Khoa, G. R. Satchler, and W. von Oertzen, Phys. Rev. C **56**, 954 (1997)
[39] K. W. Ford and J. G. Wills, Phys. Rev. **185**, 1429 (1969)
[40] W. M. Seif and H. Mansour, Int. J. Mod. Phys. E **24**, 1550083 (2015)
[41] M. {El-Azab Farid}, Z. Mahmoud, and G. Hassan, Nucl. Phys. A **691**, 671 (2001)
[42] G. Kocak, M. Karakoc, I. Boztosun, and A. B. Balantekin, Phys. Rev. C **81**, 024615 (2010)
[43] G. Satchler and W. Love, Phys. Rep. **55**, 183 (1979)
[44] R. Li, Y. Wu, and C. Xu, to be submitted.
[45] M. Dasgupta, D. J. Hinde, N. Rowley, A. M. Stefanini, Annu. Rev. Nucl. Part. Sci. **48**, 401 (1998)
[46] A. T. Kruppa, P. Romain, M. A. Nagarajan, N. Rowley, Nucl. Phys. A **560**, 845 (1991)
[47] K. Hagino, K. Ogata, A. M. Moro, Prog. Part. Nucl. Phys. **125**, 103951 (2022)
[48] A. Shrivastava, A. Navin, A. Diaz-Torres, V. Nanal, K. Ramachandran, M. Rejmund, S. Bhattacharyya, A. Chatterjee, S. Kailas, A. Lemasson, *et al*., Phys. Lett. B **718**, 931 (2013)
[49] A. M. Stefanini, G. Montagnoli, M. D'Andrea, M. Giacomin, C. Dehman, R. Somasundaram, V. Vijayan, L. Zago, G. Colucci, F. Galtarossa, *et al*., J. Phys. G: Nucl. Part. Phys. **48**, 055101 (2021)
[50] A. Tohsaki, H. Horiuchi, P. Schuck, and G. Röpke, Phys. Rev. Lett. **87**, 192501 (2001)
[51] H. Esbensen, Phys. Rev. C **68**, 034604 (2003)
[52] Vijay, M. S. Gautam, R. P. Chahal, S. Duhan, and H. Khatri, Phys. Scr. **97**, 045305 (2022)
[53] A. C. Visakh, E. Prasad, P. V. Laveen, M. Shareef, A. Shamlath, S. Nath, N. Madhavan, J. Gehlot, Gonika, R. Biswas, *et al*., Phys. Rev. C **104**, 054602 (2021)
[54] M. Pignanelli, N. Blasi, J. Bordewijk, R. De Leo, M. Harakeh, M. Hofstee, S. Micheletti, R. Perrino, V. Ponomarev, V. Soloviev, *et al*., Nucl. Phys. A **559**, 1 (1993)
[55] J. R. Leigh, M. Dasgupta, D. J. Hinde, J. C. Mein, C. R. Morton, R. C. Lemmon, J. P. Lestone, J. O. Newton, H. Timmers, J. X. Wei, *et al*., Phys. Rev. C **52**, 3151 (1995)
[56] A. Shrivastava, S. Kailas, A. Chatterjee, A. Navin, A. M. Samant, P. Singh, S. Santra, K. Mahata, B. S. Tomar, and G. Pollarolo, Phys. Rev. C **63**, 054602 (2001)
[57] K. Hagino, N. Rowley, and A. Kruppa, Comput. Phys. Commun. **123**, 143 (1999)
[58] T. Ichikawa, K. Hagino, and A. Iwamoto, Phys. Rev. C **75**, 064612 (2007)
[59] E. F. Aguilera, J. J. Kolata, and R. J. Tighe, Phys. Rev. C **52**, 3103 (1995)
[60] C. R. Morton, M. Dasgupta, D. J. Hinde, J. R. Leigh, R. C. Lemmon, J. P. Lestone, J. C. Mein, J. O. Newton, H. Timmers, N. Rowley, *et al*., Phys. Rev. Lett. **72**, 4074 (1994)
[61] J. O. Newton, C. R. Morton, M. Dasgupta, J. R. Leigh, J. C. Mein, D. J. Hinde, H. Timmers, and K. Hagino, Phys. Rev. C **64**, 064608 (2001)
[62] G. Duchêne, P. Romain, F. A. Beck, P. Benet, D. Disdier, B. Haas, B. Lott, V. Rauch, F. Scheibling, J. P. Vivien, *et al*., Phys. Rev. C **47**, 2043 (1993)
[63] M. Dasgupta, D. J. Hinde, A. Diaz-Torres, B. Bouriquet, C. I. Low, G. J. Milburn, and J. O. Newton, Phys. Rev. Lett. **99**, 192701 (2007)
[64] A. Shrivastava, K. Mahata, S. Pandit, V. Nanal, T. Ichikawa, K. Hagino, A. Navin, C. Palshetkar, V. Parkar, K. Ramachandran, *et al*., Phys. Lett. B **755**, 332 (2016)
[65] A. Mukherjee, D. J. Hinde, M. Dasgupta, K. Hagino, J. O. Newton, and R. D. Butt, Phys. Rev. C **75**, 044608 (2007)
[66] C. L. Jiang, B. B. Back, H. Esbensen, J. P. Greene, R. V. F. Janssens, D. J. Henderson, H. Y. Lee, C. J. Lister, M. Notani, R. C. Pardo, *et al*., Phys. Rev. C **78**, 017601 (2008)